Effects of Considering Kinematic Hardening in Stress Calculations

A. Fettahoğlu[1], S. Bekiroğlu[2]

[1]European Turkish Business Centre, Trabzon, Turkey, abdullahfettahoglu@gmail.com
[2]Department of Civil Engineering, Yıldız Technical University, Istanbul, Turkey, bekiroglu_serkan@yahoo.com

Abstract

The ductility of steel ever known as non-linear material property causes stress relief with plastic hinge formation and increases the load carrying capacity of structures made of steel can be best incorporated into stress calculations by means of Finite Element Methods (FEMs). The ductility of steel is considered in stress calculations either as a simplification in calculations or directly incorporated into calculations as non-linear material property. The phenomenon, incorporating the complex geometry of steel components and material non-linearity in stress calculations can be achieved by means of FEMs. The steel orthotropic highway bridges, which are composed of deck-plate, longitudinal stiffeners going through cross-beams, cross-beams with cut-outs, main girders, bridge extensions for pedestrians, are extremely complex in geometry and made of steel, which is ductile in nature. As a result, FEM-stress calculation of orthotropic steel bridge is a perfect example for the investigation of ductility induced stress relief. The traditional constructional details and their dimensions of steel orthotropic highway bridges are given in DIN FB-103. In the scope of this study, based on dimensions recommended in DIN FB-103 and kinematic hardening material property of steel material, a FEM-model of steel highway bridge will be prepared. Results of calculations with and without material non-linearity will be presented and compared with each other in order to demonstrate the decrease in stress because of steel ductility.

Keywords: *FEM, kinematic hardening, ductility, orthotropic steel bridges*

1 Introduction

The effect of kinematic hardening in stress calculations is evaluated using the structural geometry of steel highway orthotropic bridge. Steel highway bridges are really adequate examples for kinematic hardening, since most of these bridges are today overloaded according to their design loads. Most of these bridges were designed especially in Germany in years 1960, which have a typical cross- section shown in Figure1. From that time to so far the number and weight of vehicles passing over these bridges increased heavily, so that the load bearing parts of the bridges are subject to more loads and loaded more frequently than they are designed. To indicate the effect of kinematic hardening, which is a property of structures made of steel, the bridge FEM-model is loaded beyond its material yield point.

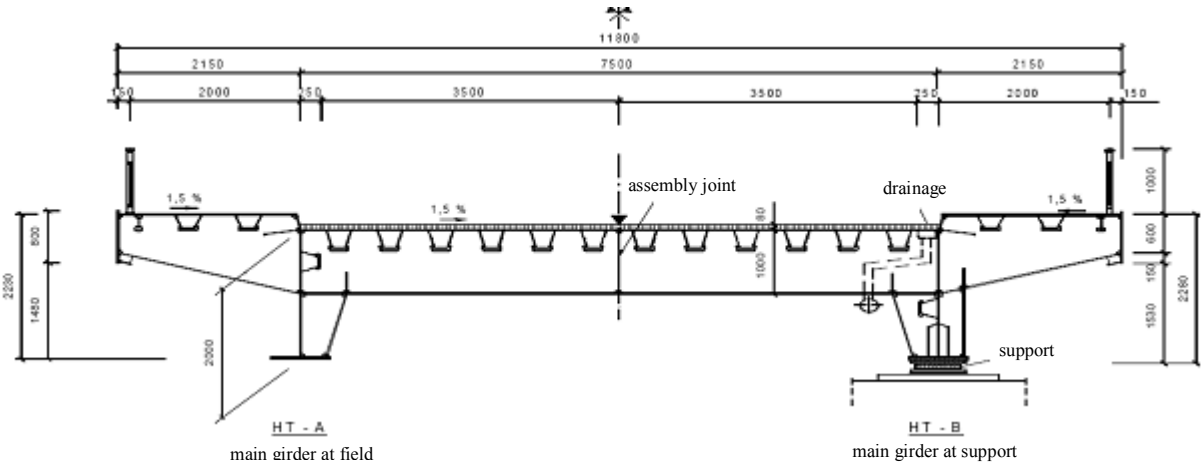


Figure 1. Typical cross- section of a steel orthotropic highway bridge.

2 FEM- Model of the Bridge

The FEM model of Huurman et.al. (2002) inspired the researchers to create FEM model of the bridge used in this research. In addition to the Huurman et.al. (2002)' s FEM-model the stiffened main girder and the pedestrian road are included in this FEM-model of bridge. As a result not the same mesh, but a similar one is used, which embraces the corner details shown in Figure 2. The comparison of two FEM-models is given in Figure 2 and 3.

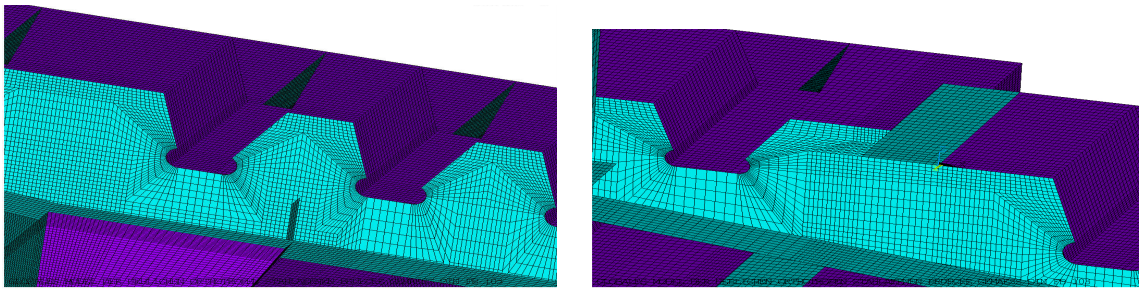


Figure 2. Left, connection of cross-beam to main girder. Right, connection of deck plate to pedestrain road.

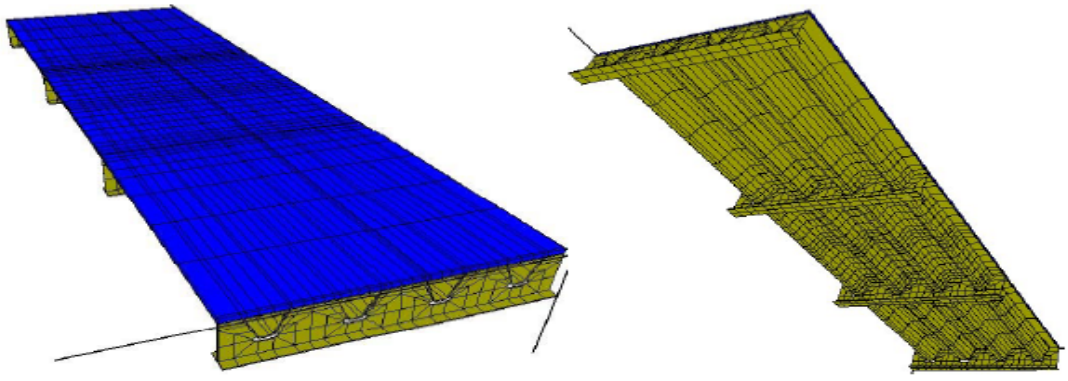


Figure 3. Huurman's FEM-model for orthotropic steel bridge.

Because of the number of nodal unknowns the dimensions of the bridge used in this research are chosen as short as possible. As a result the bridge spans 6 m and has 2 stiffened main girders at supports, 1 normal main girder at field (at the middle point), 2 exterior- 5 interior ribs and 1 rib in pedestrian road. To decrease the number of nodal unknowns further just the quarter of the bridge shown in Figure 4 is modeled by means of FEM program, ANSYS (2010).

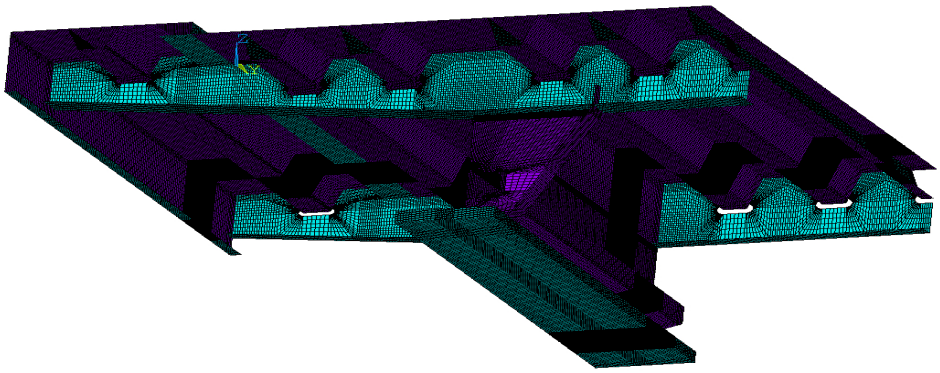


Figure 4. FEM- model of orthotropic steel bridge.

3 Geometric Nonlinearity

The finite element SHELL 181 embedded in ANSYS enables considering both geometric and material nonlinearities. In this research the geometric nonlinearity is considered using Newton Raphson Procedure. (ANSYS, 2010). The general equation of nodal unknowns are given as,

$$[K]\cdot\{u\}=\{F^a\} \tag{1}$$

whereas,

$[K]$ = Stiffness matrix,
$\{u\}$ = Displacements (nodal unknowns) vector,
$\{F^a\}$ = Load vector.

If $[K]$ is a function of $\{u\}$, Eq. (1) becomes a nonlinear equation. The Newton- Raphson- Method makes the iterative solution of nonlinear equation system possible and given as, (Bathe, 1996)

$$[K_i^T]\cdot\{\Delta u_i\}=\{F^a\}-\{F_i^{nr}\} \tag{2}$$

$$\{u_{i+1}\}=\{u_i\}+\{\Delta u_i\} \tag{3}$$

whereas,

$[K_i^T]$ = Tangential stiffness matrix,
i = Number of current iteration,
$[F_i^{nr}]$ = Vector of internal element forces derived from stresses.

$[K_i^T]$ and $[F_i^{nr}]$ are functions of $\{u_i\}$. The right side of Eq. (2) is residual- load vector. This vector is the measure of loads, which remains out of equilibrium. The first and second iterations in the method are illustrated in Figure 5 and the graphical illustrations of the method are also given step by step as follows:

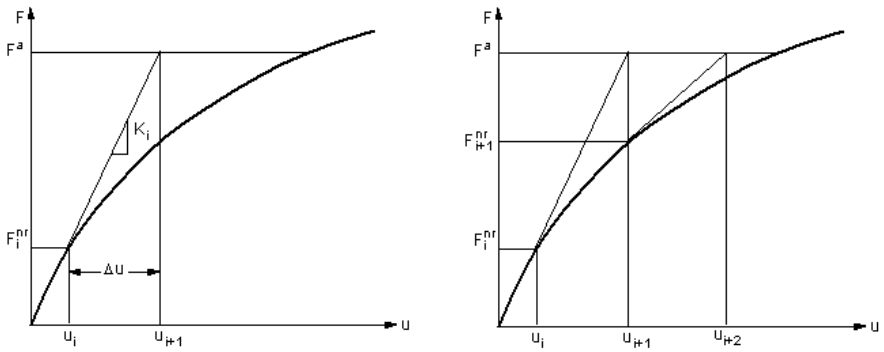


Figure 5. The Newton- Raphson- Method. First iteration (Left), second iteration (Right).

1. $\{u_0\}$ is assumed. $\{u_0\}$ is the approximate solution from previous solution ($\{u_{i-1}\}$). For the first time step, $\{u_0\} = \{0\}$.
2. The tangential stiffness matrix $[K_i^T]$ and the element forces $[F_i^{nr}]$ are calculated from the new configuration of structure $\{u_i\}$.
3. $\{\Delta u_i\}$ is calculated using Eq. (2).
4. $\{\Delta u_i\}$ is summed with $\{u_i\}$ to obtain the next solution $\{u_{i+1}\}$.
5. The steps 2 to 4 are repeated, until the convergence is correct enough.

The iterations described above keep going, unless the convergence fulfils, that is until $[F_i^{nr}]$ becomes equal to $\{F^a\}$ (In a tolerance range).

4 Material Nonlinearity

The material nonlinearity of steel is incorporated into FEM-simulations using "Bilinear-Kinematic-Hardening" law, which conforms to prEN 1993-1-5: 2004(E) Table C2.c. This theory comprises yield function, hardening and flow rules. Here just a summary of method is given, but more details can be found in Mendelson (1968), Cook (1989), and Simo and Taylor (1985). The yield criterion proposes a stress state, after which material starts to yield. This criterion is a yield function of stress tensor and equals to equivalent von Mises stress with Kinematic Hardening,

$$\sigma_e = \left[\frac{3}{2}\left(\{s\}-\{\alpha\}\right)^T [M]\left(\{s\}-\{\alpha\}\right)\right]^{1/2} \quad (4)$$

whereas,

$\{s\}$ = deviatoric stress vector

$\{\alpha\}$ = Backstress or displacement vector of yield surface.

$$\{s\} = \{\sigma\} - \sigma_m [1 \quad 1 \quad 1 \quad 0 \quad 0 \quad 0]^T = [\{s_\sigma\} \quad \{s_\tau\}]^T \quad (5)$$

$$\{\alpha\} = C\int d\{\varepsilon^{pl}\} = [\{\alpha_\sigma\} \quad \{\alpha_\tau\}]^T \quad (6)$$

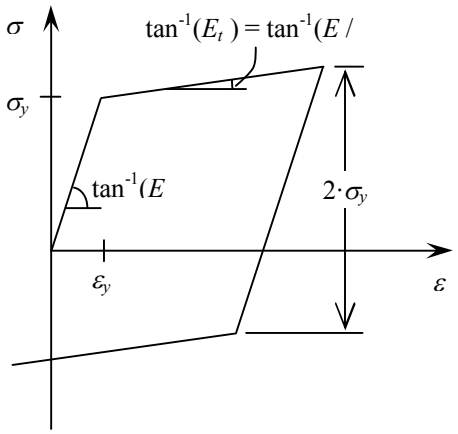


Figure 6. Stress strain relationship of steel.

The unknowns in Eq. (5) and Eq. (6) mean:

$$\{\sigma\} = \text{Stress vector} = [\sigma_x \quad \sigma_y \quad \sigma_z \quad \tau_{xy} \quad \tau_{yz} \quad \tau_{xz}]^T \quad (7)$$

$$\sigma_m = \text{Hydrostatic stress} = \frac{1}{3}\left(\sigma_x + \sigma_y + \sigma_z\right) \quad (8)$$

$$C = \frac{2}{3}\frac{E \cdot E_T}{E - E_T} \quad (9)$$

As per von Mises-yield criterion yielding does not depend on hydrostatic stress. When the equivalent stress becomes equal to the uniaxial yield stress (σ_y), the material starts to yield. As a result the yield criterion is given as,

$$F = \left[\frac{3}{2}\left(\{s\}-\{\alpha\}\right)^T [M]\left(\{s\}-\{\alpha\}\right)\right]^{1/2} - \sigma_y = 0 \quad (10)$$

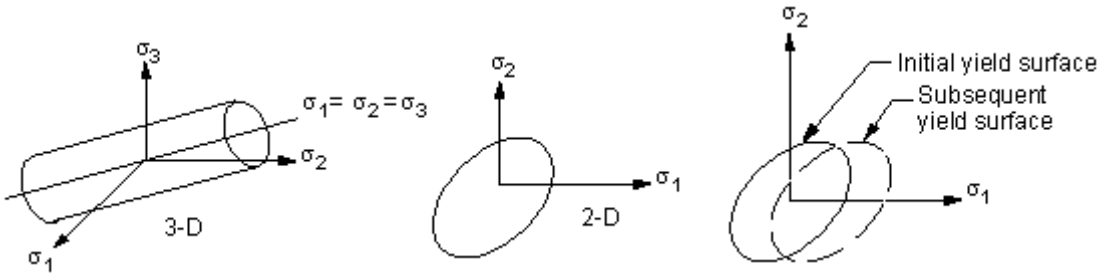


Figure 7. Yield surface according to "Kinematic Hardening".

The direction and amplitude of plastic strain are using flow rule, which is given as,

$$\{d\varepsilon^{pl}\} = \lambda\left\{\frac{\partial Q}{\partial \sigma}\right\} \tag{11}$$

Whereas,

λ = Plastic constants, which sets the value of plastic strain.
Q = Plastic potential function, which sets the direction of plastic strain.

Here Q is equal to yield function given with Eq. (10) and the plastic strain develops perpendicular to yield surface. Therefore this flow rule is called as "Associative Flow Rule". Now to be able to calculate plastic strain, λ has to be calculated. The transform of Eq. (10) results in:

$$F(\{\sigma\},\{\alpha\}) = 0 \tag{12}$$

The first derivation of yield function results in:

$$dF = \left\{\frac{\partial F}{\partial \sigma}\right\}^T [M]\{d\sigma\} + \left\{\frac{\partial F}{\partial \alpha}\right\}^T [M]\{d\alpha\} = 0 \tag{13}$$

Whereas, $$[M] = \begin{bmatrix} 1 & 0 & 0 & 0 & 0 & 0 \\ 0 & 1 & 0 & 0 & 0 & 0 \\ 0 & 0 & 1 & 0 & 0 & 0 \\ 0 & 0 & 0 & 2 & 0 & 0 \\ 0 & 0 & 0 & 0 & 2 & 0 \\ 0 & 0 & 0 & 0 & 0 & 2 \end{bmatrix} \tag{14}$$

from Eq. (6) results $\{d\alpha\}$ in,

$$\{d\alpha\} = C\{d\varepsilon^{pl}\} \tag{15}$$

The increment of stresses can be calculated using the relationship between elastic stresses and strains.

$$\{d\sigma\} = [D]\{d\varepsilon^{el}\} \tag{16}$$

$$\{d\varepsilon^{el}\} = \{d\varepsilon\} - \{d\varepsilon^{pl}\} \tag{17}$$

whereas,

[D] = Stresss-Strain Matrix
ε^{el} = Elastic Strains

ε^{pl} = Plastic Strains
When Eq. (15) and Eq. (16) with Eq. (17) are replaced in Eq. (13), it is obtained,

$$\left\{\frac{\partial F}{\partial \sigma}\right\}^T [M][D]\{d\varepsilon\} = \left(-C\left\{\frac{\partial F}{\partial \alpha}\right\}^T [M] + \left\{\frac{\partial F}{\partial \sigma}\right\}^T [M][D]\right)\left\{d\varepsilon^{pl}\right\} \tag{18}$$

In Eq. (18) $\left\{d\varepsilon^{pl}\right\}$ is replaced with Eq. (11) under consideration of equation, $Q = F$.

$$\lambda = \frac{\left\{\frac{\partial F}{\partial \sigma}\right\}^T [M][D]\{d\varepsilon\}}{-C\left\{\frac{\partial F}{\partial \alpha}\right\}^T [M]\left\{\frac{\partial F}{\partial \sigma}\right\} + \left\{\frac{\partial F}{\partial \sigma}\right\}^T [M][D]\left\{\frac{\partial F}{\partial \sigma}\right\}} \tag{19}$$

Therefore the increment in plastic strains depends on the total strain increment, the current stress state and the form of yield function. Subsequently, λ can be calculated and the plastic strain increment results using Eq. (11) in,

$$\left\{\frac{\partial F}{\partial \sigma}\right\} = \left(\frac{3}{2 \cdot \sigma_y}\begin{bmatrix}\{s_\sigma\} - \{\alpha_\sigma\} \\ 0\end{bmatrix} + \frac{3}{\sigma_y}\begin{bmatrix}0 \\ \{s_\tau\} - \{\alpha_\tau\}\end{bmatrix}\right) \tag{20}$$

The algorithm is as follows:

1. The stresses are calculated based on a test strain $\{\varepsilon^{tr}\}$, which is the total strain minus the plastic strain from the previous time point.

   $$\left\{\varepsilon_n^{tr}\right\} = \left\{\varepsilon_n\right\} - \left\{\varepsilon_{n-1}^{pl}\right\} \tag{21}$$

   n stands for the current time point. Then the test stress yields in,

   $$\left\{\sigma_n^{tr}\right\} = [D]\left\{\varepsilon_n^{tr}\right\} \tag{22}$$

2. Using Eq. (4) the equivalent stress is calculated. If σ_e smaller than σ_y is, material behaves like elastic and no calculation of plastic strain increment is required.
3. As long as the equivalent stress the yield point excesses, λ is calculated using Local-Newton-Raphson-Iteration-Process Simo and Taylor (1985).
4. $\left\{\Delta\varepsilon^{pl}\right\}$ is calculated using Eq. (11).
5. The current plastic strain is calculated.

   $$\left\{\varepsilon_n^{pl}\right\} = \left\{\varepsilon_{n-1}^{pl}\right\} + \left\{\Delta\varepsilon^{pl}\right\} \tag{23}$$

   Subsequently the elastic strain is calculated.

   $$\left\{\varepsilon^{el}\right\} = \left\{\varepsilon^{tr}\right\} - \left\{\Delta\varepsilon^{pl}\right\} \tag{24}$$

   Consequently the stress vector is again calculated using elastic strains and then the iterations are repeated until the convergence is satisfied.

   $$\{\sigma\} = [D]\left\{\varepsilon^{el}\right\} \tag{25}$$

6. The difference in position of yield surface is calculated using Eq. (15), whereas n-1 depends on the value of previous time point.

$$\{\alpha_n\} = \{\alpha_{n-1}\} + \{\Delta\alpha\} \tag{26}$$

5 Bridge Loads as per DIN FB 101

5.1 Material Properties of Steel

The selected steel material is S 355. According to Capital II of DIN FB 103 the yield stress and strength values are given in Table 1. According to Capital III of DIN FB 101 and E- DIN 1055- 1: 2000 a distributed load of 0.24 kN/ m² per cm of asphalt course, which lies on deck plate, is applied.

Table 1. Material properties.

Yield strength of steel (f_y)	355 N/mm^2	Shear module (G)	81,000 N/mm^2
Ultimate strength (f_u)	510 N/mm^2	Poisson ratio (υ)	0,3
Elasticity module (E)	210,000 N/mm^2	Density (ρ_{steel})	78.5 kN/m^3

5.2 Traffic Loads

The traffic load group 1 is applied on the bridge according to Capital IV of DIN FB 101. The traffic road, on which vehicles pass, are divided into numerical traffic lanes, which has the properties given in Table 2.

Table 2. Properties of traffic lanes.

Road width (w)	6.3 m	Number of numerical traffic lanes (n_1= Int(w /3))	2
Width of numerical traffic lanes (w_1)	3.0 m	Width of remaining surface within of road ($w_R = w - w_1 \cdot n_1$)	0.3 m

Traffic road consists of two numerical traffic lanes, which have 3m width and are under traffic loading. According to DIN FB 101 traffic load group 1 comprises characteristic load values of dominant load model 1 and reduced values of pedestrian loads. Here loading is chosen to be applied at symmetry planes, so that no loading of pedestrian loads are inconvenient. As a result no pedestrian load is considered in the FEM- model of the bridge. The load values are given in table 3.

Table 3. Properties of traffic loads.

Wheel load on main traffic lane	180 kN	Weight of asphalt course per cm asphalt thickness	0.324 kN/m²
Equally distributed load on main traffic lane	13.5 kN/ m²	Density (ρ_{steel})	105.975 kN /m³

6 Optimization of Mesh and Substeps

The optimization of mesh refinement and substeps are done under traffic load group 1 according to DIN FB 101 for limit state of load carrying capacity. In addition asphalt course thickness is taken as 75 mm. Therefore the wheel load area is expanded from 0.4x0.4 m^2 to 0.562x0.562 m^2. (Here 0.562 m = 0.4 m (width of wheel area) + 2*0.075 m (thickness of asphalt) + 2*0.006 m (half of deck plate thickness)). However because of the limitation caused by finite elements' side-sizes in model, the width of wheel area has to be any times of 75 mm. Subsequently, the width of wheel load area is set as 0.525 m. The traffic loading is illustrated in Figure 8.

Here searched the optimal mesh refinement for FEM-model of bridge. Two criteria are important for this issue. First the correctness of results, second number of elements, nodal unknowns, iterations and time takes during simulation. At the beginning mesh refinement is chosen with experience. Since the number of solution substeps and mesh refinement are separately analyzed, geometric and material non-linearities are ignored in mesh refinement analyses. Under these assumptions five simulations are performed and Table 4 is produced. From assessment of Table 4 Mesh 4 is chosen as adequate mesh for FEM-model of bridge.

Except **SXY_MIN (**min. σ_{xy}**)**, **EPTOXY_MIN (**min. ε_{xy}**)** developed in the rib of main girder, and **SYZ_MIN (**min. σ_{yz}**)** , **EPTOYZ_MIN (**min. ε_{yz}**)** developed in the bottom flange of main girder web, all deviations between Mesh 4 and Mesh 5 are smaller than 6 %. Moreover all stress vales are much smaller than yield stress. As a result Mesh 4 provides stresses and strains within enough tolerance for this research.

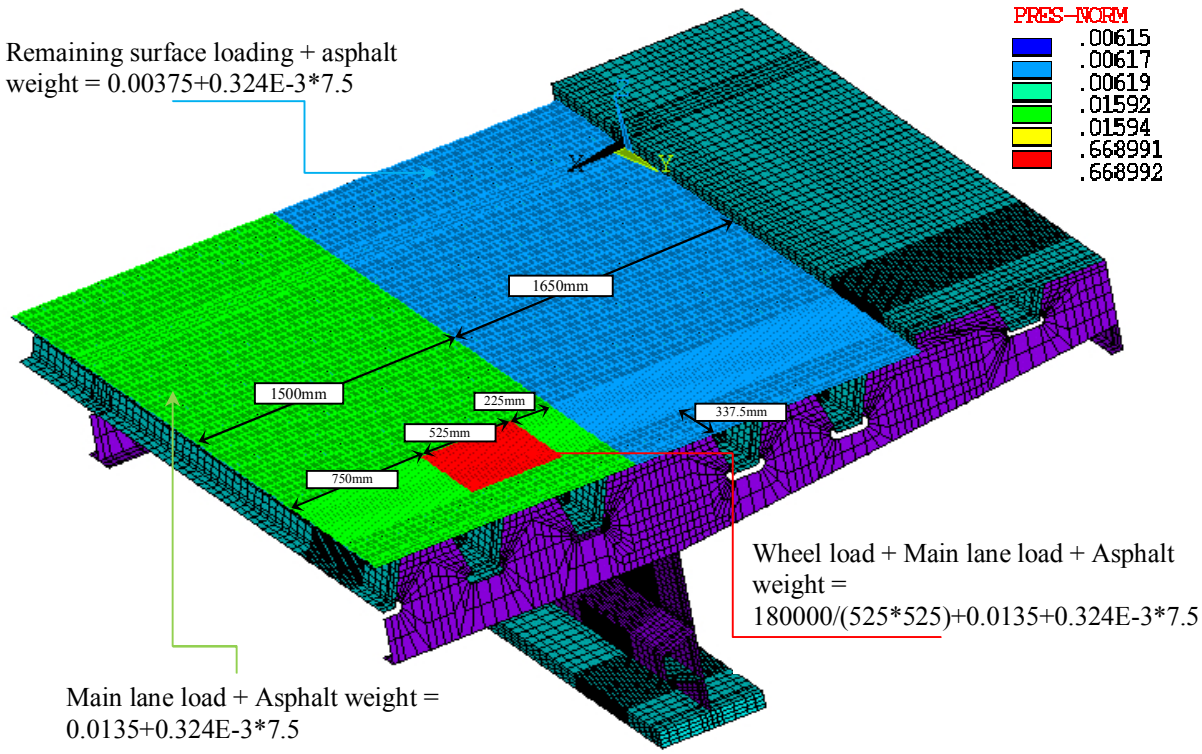


Figure 8. Traffic loading used for parameter study.

Table 4. Number of elements, stresses and strains as per mesh refinement*

		Mesh 1	Mesh 2	Mesh 3	Mesh 4	Deviation (%) between Mesh 4 and 5	Mesh 5
Number of elements		29194	123288	197300	**300282**	49.27	448217
UMAX		3.276	3.313	3.318	**3.324**	0.06	3.326
SEQV		340.811	447.555	474.723	**493.657**	3.49	510.907
SX	**MIN**	-149.676	-191.998	-202.247	**-217.881**	3.32	-225.115
	MAX	211.383	283.732	300.268	**311.536**	2.56	319.505
SY	**MIN**	-175.329	-200.493	-204.560	**-221.599**	1.22	-224.298
	MAX	104.559	154.831	159.656	**188.834**	1.38	191.435
SZ	**MIN**	-372.416	-474.806	-501.148	**-517.904**	2.09	-528.745
	MAX	225.191	296.616	314.405	**347.377**	3.19	358.470
SXY	**MIN**	-29.838	-38.785	-44.041	**-55.47**	7.54	-59.655
	MAX	34.205	39.335	40.003	**41.638**	3.77	43.206
SYZ	**MIN**	-44.871	-49.162	-50.44	**-66.276**	9.00	-72.243
	MAX	69.991	82.527	84.422	**91.290**	0.60	91.838
SXZ	**MIN**	-116.337	-158.462	-173.985	**-184.413**	4.80	-193.263
	MAX	90.568	107.776	116.876	**123.881**	5.88	131.165
EPTOEQV		0.001623	0.002131	0.002261	**0.002351**	3.49	0.002433
EPTOX	**MIN**	-0.000665	-0.000850	-0.000897	**-0.000961**	3.33	-0.000993
	MAX	0.000798	0.001131	0.001222	**0.001289**	3.57	0.001335
EPTOY	**MIN**	-0.000812	-0.000860	-0.000863	**-0.000902**	0.33	-0.000905
	MAX	0.000671	0.000808	0.000856	**0.000881**	1.36	0.000893
EPTOZ	**MIN**	-0.001641	-0.002137	-0.002271	**-0.002359**	2.50	-0.002418
	MAX	0.001091	0.001409	0.001482	**0.001613**	2.85	0.001659
EPTOXY	**MIN**	-0.000369	-0.000480	-0.000545	**-0.000687**	7.57	-0.000739
	MAX	0.000423	0.000487	0.000495	**0.000516**	3.68	0.000535
EPTOYZ	**MIN**	-0.000556	-0.000609	-0.000625	**-0.000821**	8.89	-0.000894
	MAX	0.000867	0.001022	0.001045	**0.001130**	0.62	0.001137
EPTOXZ	**MIN**	-0.00144	-0.001962	-0.002154	**-0.002283**	4.82	-0.002393
	MAX	0.001121	0.001334	0.001447	**0.001534**	5.87	0.001624

* The symbols used in table are:

SEQV = σ_e, **SX** = σ_x, **SY** = σ_y, **SZ** = σ_z, **SXY** = σ_{xy}, **SYZ** = σ_{yz}, **SXZ** = σ_{xz},

EPTOEQV = ε_e, **EPTOX** = ε_x, **EPTOY** = ε_y, **EPTOZ** = ε_z, **EPTOXY** = ε_{xy}, **EPTOYZ** = ε_{yz}, **EPTOEXZ** = ε_{xz}

Number of substeps is chosen as 5, 8 and 10 and simulations are done using Mesh 4. Assessment of these results emerges that even 5 substep number is enough to obtain results in convergence tolerance. Anyway in this research results with 8 substep number are used to display the results in Table 5.

Table 5. Stresses and strains as per number of substeps

		Simulation 1	Deviation(%) between Simulation 1 and 2	Simulation 2	Deviation(%) between Simulation 2 and 3	Simulation 3
Number of Substeps		5	60	**8**	25.00	10
Number of Iterations		16	19	**19**	26.32	24
UMAX		3.344	0.00	**3.344**	0.00	3.344
SEQV		404.026	0.00	**404.010**	0.00	404.005
SX	**MIN**	-219.675	0.00	**-219.676**	0.00	-219.676
	MAX	311.243	0.00	**311.230**	0.00	311.226
SY	**MIN**	-220.591	0.00	**-220.591**	0.00	-220.592
	MAX	189.223	0.00	**189.225**	0.00	189.226
SZ	**MIN**	-401.416	0.01	**-401.441**	0.00	-401.451
	MAX	343.998	0.00	**343.994**	0.00	343.994
SXY	**MIN**	-55.020	0.00	**-55.020**	0.00	-55.020
	MAX	41.899	0.00	**41.899**	0.00	41.899
SYZ	**MIN**	-66.229	0.00	**-66.228**	0.00	-66.228
	MAX	90.386	0.00	**90.386**	0.00	90.386
SXZ	**MIN**	-184.727	0.00	**-184.720**	0.00	-184.717
	MAX	122.590	0.00	**122.589**	0.00	122.588
EPTOEQV		0.002572	0.12	**0.002569**	0.16	0.002565
EPTOX	**MIN**	-0.000969	0.00	**-0.000969**	0.00	-0.000969
	MAX	0.001289	0.00	**0.001289**	0.00	0.001289
EPTOY	**MIN**	-0.000899	0.00	**-0.000899**	0.00	-0.000899
	MAX	0.001241	0.89	**0.001230**	0.00	0.001230
EPTOZ	**MIN**	-0.002554	0.20	**-0.002549**	0.00	-0.002549
	MAX	0.001597	0.00	**0.001597**	0.00	0.001597
EPTOXY	**MIN**	-0.000681	0.00	**-0.000681**	0.00	-0.000681
	MAX	0.000519	0.00	**0.000519**	0.00	0.000519
EPTOYZ	**MIN**	-0.000820	0.00	**-0.000820**	0.00	-0.000820
	MAX	0.001119	0.00	**0.001119**	0.00	0.001119
EPTOXZ	**MIN**	-0.002287	0.00	**-0.002287**	0.00	-0.002287
	MAX	0.001518	0.00	**0.001518**	0.00	0.001518

7 Results

The results obtained neglecting non-linearities shows that the non-linearity has to be considered in the simulation, since some stress values excess the yield point (355 MPa). Figure 9 displays the effect of considering kinematic hardening in stress calculations. Figure 9 presents the results of hardening. According to solution neglecting kinematic hardening the structure fails at some points. However considering kinematic hardening in stress calculations proves that the structure does not fail and continues to carry load thanks to ductile material property of steel, while plastic strains develop. While local vertical displacement under wheel load and von Mises strain increase 0.60 % and 9.27 % respectively, von Mises stress decreases 18.16 %. The plastic strain develops just in the joint between cross- beam and longitudinal rib as shown in Figure 10.

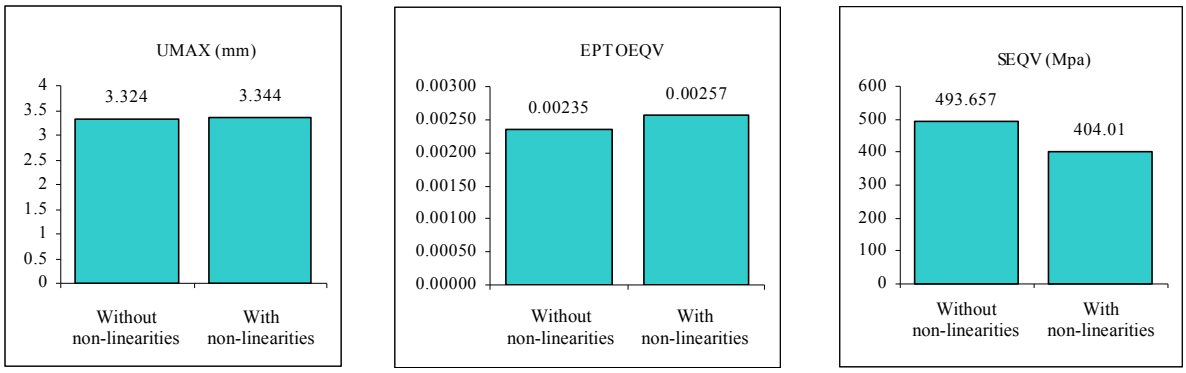


Figure 9. Effect of considering kinematic hardening in stress calculations.

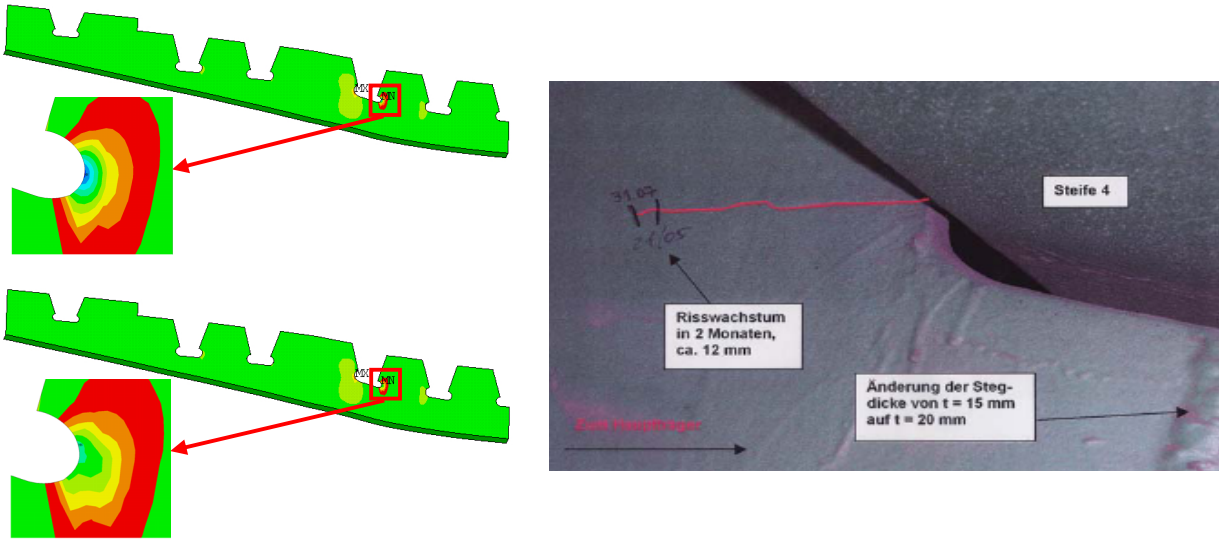


Figure 10. Top left, distribution of **SZ** on cross- beam with neglecting nonlinearity, bottom left, with considering nonlinearity, right the yield line on the material emerged in an orthotropic steel bridge.

References

ANSYS (2010). *User Manuals*. Swanson Analysis System. USA.

Bucak, Ö. (2005). *Reparatur durch Stegauspflasterung*. Manuskript zum Expertengespräch Instandsetzung orthotroper Fahrbahnplatten, Bundesanstalt für Strassenwesen, Bergisch Gladbach.

Cook, D.R., Malkus, D.S. and Plesha, M.E. (1989) *Concepts and Applications of Finite Element Analysis*. John Wiley & Sons- Press. New York.

DIN FB 101 (2003). *Einwirkungen auf Brücken*. Deutsches Institut für Normung. Berlin.

DIN FB 103 (2003). *Stahlbrücken*. Deutsches Institut für Normung. Berlin.

E- DIN 1055- 1 (2000). *Lastannahmen für Bauten*. Berlin.

Fettahoğlu A., Bekiroğlu, S. (2012, October). *Effect of Deck Plate Thickness on the Structural Behavior of Steel Orthotropic Highway Bridges*. Paper presented at meeting of the Advanced in Civil Engineering, Ankara, Turkey

Huurman et.al. (2002). 3D-FEM for the estimation of the behaviour of asphaltic surfacings on orthotropic steel deck bridges. *3rd International Symposium on 3D Finite Element for Pavement Analysis, Design & Research*, Amsterdam.

Mendelson, A. (1968). *Plasticity: Theory and Application*. The Macmillan Company. New York.

prEN 1993-1-5 (2004). *Bemessung und Konstruktion von Stahlbauten. Aus Blechen zusammengesetzte Bauteile*. Brussel.

Simo, J. C. and Taylor, R.L. (1985). Consistent Tangent Operators for Rate-Independent Elastoplasticity. *Computer Methods in Applied Mechanics and Engineering*. Vol. 48, pp. 101- 118.